Journal of The Electrochemical Society, **163** (1) A5057-A5063 (2016)
0013-4651/2016/163(1)/A5057/7/$33.00 © The Electrochemical Society

JES Focus Issue on Redox Flow Batteries—Reversible Fuel Cells

Cycling Analysis of a Quinone-Bromide Redox Flow Battery

Qing Chen,[a] Louise Eisenach,[b] and Michael J. Aziz[a,*,z]

[a]*Harvard John A. Paulson School of Engineering and Applied Sciences, Cambridge, Massachusetts 02137, USA*
[b]*Harvard College, Cambridge, Massachusetts 02138, USA*

We report the dependence upon current density of voltage polarization; charge capacity; and current, voltage, and energy efficiency for a flow battery comprising 2,7-anthraquinone disulfonic acid and hydrobromic acid as redox-active species in the electrolytes. We develop relationships predicting several of these figures of merit from the polarization curves. The decrease in capacity with increasing current density is shown to be a direct consequence of the interplay of the polarization curves and the voltage limits imposed during cycling. The linearity of the polarization curves results in an inverse linear relationship between instantaneous voltage efficiency and current density. The average voltage efficiency over a complete cycle is shown to follow this same relationship when the open-circuit voltage and polarization resistance are evaluated at 50% state of charge. Current efficiency loss mechanisms are classified according to whether they lead directly to cycle capacity loss. The current efficiency increases with current density due to constant-rate loss mechanisms at a rate of 1.08 mA/cm^2, which is consistent with the rate of bromine crossover. Quinone crossover is negligible at 140 pA/cm^2. The effective differential capacity retention rate is 99.90% per cycle over 40 cycles. Mechanistic interpretations for these results are offered and interrelationships derived.

Manuscript submitted June 16, 2015; revised manuscript received August 28, 2015. Published September 16, 2015. *This paper is part of the JES Focus Issue on Redox Flow Batteries–Reversible Fuel Cells.*

The greatest technical obstacle to deep penetration of photovoltaics and wind into our electricity mix is their intermittency. Cost-effective bulk electricity storage, e.g. at or near renewable electricity generation sites on the electric grid, should enable stable grid operation despite the fluctuations contributed by intermittent sources. Pumped hydroelectric energy storage and underground compressed air energy storage have geographical limitations as well as other disadvantages. Electrochemical storage via banks of batteries is consequently receiving greatly increased attention. Traditional, enclosed batteries have limited energy-to-power ratios, which raises costs when required discharge durations can be well in excess of an hour. Unlike enclosed batteries, redox flow batteries (RFBs) store the energy in tanks of chemicals outside the cell itself. This enables the designer to independently size the power capacity (electrode area) and energy capacity (tank size), thereby permitting the relatively inexpensive increase of discharge duration by simply increasing the size of the storage tanks. The all-vanadium RFB is currently the most technologically mature system, but the high cost and low abundance of vanadium limit the scale of potential deployment of this chemistry. A great deal of effort has been devoted to the quest for a high-performance cell utilizing alternative RFB chemistries composed entirely of inexpensive materials,[1–4] as well as hybrid flow/non-flow batteries.[5–7] One promising candidate is the aqueous quinone-bromide flow battery (QBFB), which pairs a novel quinone/hydroquinone couple on the negative electrode with a conventional bromine/hydrobromic acid couple on the positive electrode.[1,2]

To compare a new RFB chemistry and cell build to existing systems, one needs to investigate properties such as open-circuit voltage (OCV); specific charge capacity; polarization overvoltage vs. current density; cycle efficiency of current, voltage, and energy; and capacity retention during cycling. The first three can be evaluated within a single charge-discharge cycle via common protocols. The remaining properties, however, require cycling at a variety of current densities spanning the range of potential usage. Consequently, only a few different current densities—and sometimes only a single value—are typically chosen for investigation of cell cycling performance. This not only leads to disparity among the chemistry and build comparisons, but also leaves open the question of cell behavior at unexamined current densities, which can be frequently encountered in actual use. It is theoretically feasible to predict many cycling characteristics of a RFB, including current, voltage, and energy efficiency, by analyzing short-period tests such as polarization. Here we use the QBFB to demonstrate this capability. We show that the behavior in a charge-discharge cycle and its dependence upon current density follows from measurements of the polarization curve at various states of charge (SOC) in the same cell. We expect that this approach can be applied to other RFB builds or systems so as to provide insights into their performance under unexamined conditions. We also measure and analyze current efficiency and capacity retention rates, and propose interpretations in terms of the dominant loss mechanisms. These analyses are intended to permit future engineering improvements to cell performance.

Experimental

The QBFB build, illustrated in Fig. 1a, is adapted from a design described previously.[1] On each side, a commercial graphite plate with interdigitated flow channels (Fuel Cell Tech, Albuquerque, NM) was used to feed electrolyte to a stack of 6 sheets of Toray 060 carbon paper, each of 5 cm^2 geometric area. No electrocatalyst was added to the carbon papers. The two sides were separated by a sheet of Nafion 115 (~125 μm), pre-soaked in DI water. A March centrifugal pump circulated the positive electrolyte (posolyte) and a MasterFlex (Cole Parmer) diaphragm pump was used for the negative electrolyte (negolyte) in order to minimize the required volume. Both electrolytes circulated at a rate of 200 mL/min. The cell operated at approximately 30°C. Assembled fully discharged, the negolyte (25 mL) contained 1 M 9,10-anthraquinone-2,7-disulfonic acid (AQDS), ion exchanged from its sodium salt (TCI) and 1 M H_2SO_4, and the posolyte (120 mL) contained 3.5 M hydrobromic acid and 0.5 M Br_2. The nominal reactions during the charging process on each side are as follows:

$$\mathrm{AQDS} + 2H^+ + 2e^- \rightarrow H_2\mathrm{AQDS}$$

$$2\mathrm{Br}^- - 2e^- \rightarrow \mathrm{Br}_2$$

Because we are primarily interested in examining the behavior of the new negolyte, we provided excessive active species, in both oxidized and reduced form, to the positive side so that the ratio of positive to negative charge capacity was 5/36. Hence we define both the theoretical capacity and SOC by the properties of the negative side. Constant-current cycling tests were carried out with voltage limits at 0 and 1.3 V (Fig. 1b), controlled by a Gamry 30k booster connected to a Gamry Reference 3000 potentiostat. The cell was cycled at each value of the current for at least 5 cycles; there were 40 cycles in total.

*Electrochemical Society Active Member.
[z]E-mail: maziz@harvard.edu

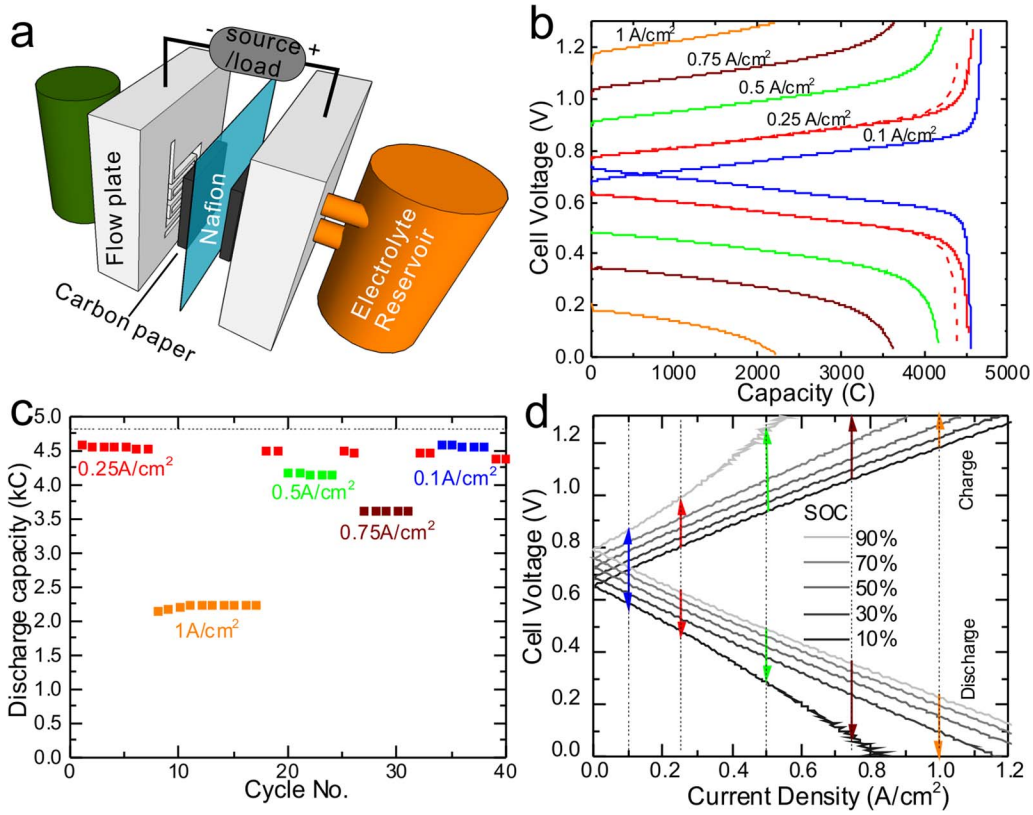

Figure 1. (a) Cell configuration. (b) Cell voltage vs. capacity for charge and discharge. Solid curves: in the 2nd cycle at each value of the current density; dashed curves: for the final cycle at 0.25 A/cm^2. (c) Discharge capacity vs. cycle number. (d. Polarization curves at various SOC; curves at even multiples of 10% SOC are hidden for clarity. Color codes for all applied current densities remain the same in b-d.

The theoretical capacity of the cell containing 25 mL of negolyte is 4824 C, assuming two electrons per molecule. We use 0.25 A/cm^2 as the base current density to evaluate the capacity retention. The cycles in which current changes occurred are excluded from the analysis. Current efficiency was evaluated as the ratio of discharging duration to immediately preceding charging duration at the same current. The round-trip energy efficiency was derived from the ratio of discharging to immediately-preceding charging energy, obtained by integrating the curves in Fig. 1b. We obtained the average voltage efficiency over a cycle by dividing the energy efficiency by the current efficiency. Polarization curves were measured via linear sweeping at a rate of 100 mV/s for SOC values from 10% to 90% in increments of 10%. We find that this sweep rate yields the same results as potentiostatic or galvanostatic holding tests in our experimental setup, yet without significantly changing the SOC of the relatively small volume of electrolytes used in the tests.

Bromine crossover was measured in the same cell with 3 M sulfuric acid in the negative reservoir against the positive electrolyte used in the cycling. 0 V was applied to the cell until a steady-state reduction current was reached. AQDS crossover was measured in a custom-built crossover cell. A sheet of Nafion 115 membrane was sandwiched between two glass chambers with an O-ring seal. A solution of 1 M AQDS and 1 M sulfuric acid in one chamber served as a source of AQDS for the other, which contained 3 M sulfuric acid. The cell was kept on a nutating mixer. The AQDS concentration in the receiving side was monitored via UV-Vis spectrophotometry based on the extinction coefficient at 325 nm.

Results

Charging and discharging curves in the second cycle at each current density are plotted in the form of cell voltage vs. capacity in Fig. 1b, and the discharge capacities of each cycle are plotted against the cycle number in Fig. 1c. The polarization curves are plotted in Fig. 1d as cell voltage vs. the absolute value of the current density. Most curves appear linear in the examined voltage range, indicating that they are dominated by resistive components in the cell—including the membrane, the electrodes and the electrolytes. Relevant area-specific resistance values are discussed elsewhere.[8]

Filled symbols in Fig. 2 show key performance metrics versus cycling current density, including the average discharge capacity, the current efficiency (CE), the voltage efficiency (VE) and the round-trip energy efficiency (EE). All figures of merit other than the CE increase with decreasing cycling current density. In Fig. 2a, the discharge capacity goes from~45% of the theoretical capacity at 1 A/cm^2 to a plateau at ~95% of the theoretical capacity at low current density. The CE and VE are both plotted in Fig. 2b, referred to the stretched left hand axis and the right hand axis respectively. The product of the two efficiencies yields the EE as plotted in Fig. 2c. Over the range of current density examined experimentally, the EE is dominated by the VE, displaying a monotonic decrease with increasing current density.

The current efficiency loss exhibits inverse linear dependence on the current density i. The black curve in Fig. 2b is a plot of

$$\mathrm{CE}\,(i) = 1 - \frac{B}{i}, \qquad [1]$$

where the adjustable parameter $B = 2.16$ mA/cm^2. A mechanistic interpretation of B is offered in the next section.

We also evaluate the capacity loss rate over the experiment by comparing the discharge capacity difference between the first and the last cycles (red curves in Fig. 1b). Because the change in capacity in each cycle is small and is within the measurement error, we evaluate only the average capacity loss rate over the entire $N = 40$-cycle regimen. Let $i_1 A t_1$ be the charge delivered at current density i_1 during

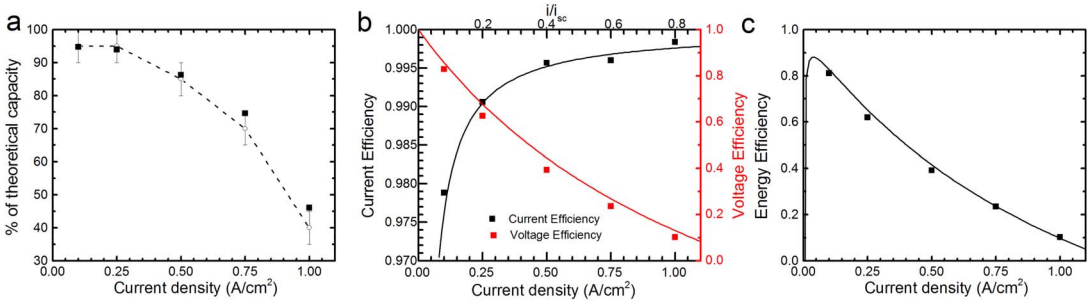

Figure 2. Cell cycling performance summary. (a) Average percentage of theoretical capacity retrieved during discharging at each current density. Filled symbols: experimental results. Open symbols with error bars, connected by line represent the values estimated from the analysis of Fig. 1d. (b) Average current and voltage efficiencies vs. current density. Smooth lines are calculated values as discussed in the text. Top axis is current density normalized by short-circuit current density at 50% SOC for correlating VE to i/i_{sc}. (c) Round-trip energy efficiency vs. current density.

the first discharge half-cycle occurring over a duration t_1, and $i_N A t_N$ be the charge delivered at current density i_N during the N^{th} discharge half-cycle occurring over a duration t_N. We define the average capacity loss equivalent current density $\bar{i}_{CL}$ as

$$\bar{i}_{CL} = \frac{(i_1 t_1 - i_N t_N)}{t_{tot}}, \qquad [2]$$

where A is the geometric area of the membrane-electrode assembly, and t_{tot} is the total cycling experiment duration comprising N complete cycles. With $A = 5$ cm^2, $i_1 = i_N = 0.25$ A/cm^2, $t_1 = 3622$ s, $t_N = t_{40} = 3517$ s and $t_{tot} = 60$ hours, we obtain an average capacity loss equivalent current density of $\bar{i}_{CL} = 0.12$ mA/cm^2. In the next section we discuss the mechanisms potentially contributing to $\bar{i}_{CL}$.

Discussion

Capacity vs. current density.— We first analyze the capacity vs. current density behavior of the cell based on the polarization curves. In Fig. 1d, vertical dashed lines are drawn at the current density values of the cycling experiments and, for illustrative purposes, the arrows are drawn to represent the voltage the cell would assume on trajectories between 10% and 90% SOC values. An arrow ending at the top (bottom) axis indicates that charging (discharging) will terminate at the imposed voltage limit before a SOC of 90% (10%) is reached. Consequently, cycles at 0.75 A/cm^2 are confined between ~10 and 80% SOC and 1.0 A/cm^2 cycles are confined between 20% and 60%. The capacity that can be utilized is then limited to ~70 and 40% of the theoretical values at these two current densities, respectively. This protocol of estimating cycling capacity vs. current density, plotted in Fig. 2a as open circles connected by a line, yields good agreement with the experimental results. Thus, the primary reason for the drop in capacity with increasing current density is that the cell does not complete a half cycle before encountering the voltage limit. We note that the error bar here is set to 5% because the polarization curves were evaluated for SOCs in multiples of 10%; this can be improved by measuring polarization curves at intermediate values of SOC. The plateau at ~95% of the theoretical capacity at low current density may originate from a combination of factors including a discrepancy between the theoretical and maximum capacities obtained experimentally; self-discharge mechanisms, which will be discussed later; and mass transport limitations. We note that the very small size of the reservoirs on our experimental cell makes the time constant for equilibration between the reservoirs and the electrodes negligible, unlike in scaled-up batteries.

Voltage efficiency and energy efficiency.— The voltage efficiency results in Fig. 2d can also be predicted from the polarization curves (Fig. 1d) observed over a wide range of SOC. The overvoltage at given charge/discharge current density can be readily approximated by fitting the measured polarization curve to a straight line, whose fitted slope we call the polarization resistance (r_p, in Ωcm^2). The voltage efficiency (VE) at a given current density (i, in A/cm^2) can be calculated as

$$VE = \frac{V_{oc} - i r_p}{V_{oc} + i r_p} \qquad [3]$$

where V_{oc} is the SOC-dependent OCV. To estimate an average voltage efficiency, $\overline{VE}$, over a charge-discharge cycle that is symmetric around 50% SOC and compare it to the experimental results in Fig. 2b, we hypothesize that Eq. 3 equally well describes $\overline{VE}$ when we insert the values of r_p and V_{oc} values at 50% SOC. This is reasonable because both the polarization curves and the charge-discharge curves are symmetrical with respect to the state of charge. The values of r_p and V_{oc} at 50% SOC are 0.56 Ωcm^2 and 0.73 V respectively. The result of this calculation, plotted as a red line in Fig. 2b, agrees very well with the average values obtained from cycling. This implies that short-period polarization tests can indeed be applied to evaluate the cell's voltage efficiency upon cycling. Clearly the analysis in this simple form is limited to linear polarization behavior. But, as it is a result of rapid (or well-catalyzed) kinetics and fast mass transport, it should not be unique to the QBFB. In fact, similar behavior has been reported in vanadium RFBs on optimized electrodes with sufficient mass transport.[9,10] Moreover, for a RFB that loses polarization linearity to a mass transport limitation, Eq. 3 should still apply when the applied cycling current remains within the linear part of the polarization behavior. To generalize the result, we can rewrite Eq. 3 as

$$VE = \frac{2}{1 + \frac{i}{i_{SC}}} - 1 \qquad [4]$$

where $i_{sc} = V_{oc}/r_p$ is the short-circuit current density. The voltage efficiency is thus a function only of the ratio of applied current to short-circuit current. As above, we assume that Eq. 4 applies equally well to $\overline{VE}$ when i_{sc} is evaluated at 50% SOC (1.3 A/cm^2). The result is the red curve in Fig. 2b referring the abscissa to the top axis. Apparently, if one wishes to maintain $\overline{VE} \geq 0.9$ or $\overline{VE} \geq 0.8$ then the applied current density cannot exceed approximately 6% or 11% of i_{sc}, respectively.

The evaluation of the energy efficiency is readily apparent from the product of Equations 1 and 3, and the result is plotted as the line in Fig. 2c. In the experiments reported here, the energy efficiency closely follows the voltage efficiency. But we predict a maximum at ~0.04 A/cm^2, below which the losses become dominated by current efficiency losses. Such behavior has been observed in hydrogen-bromine flow cell research.[13]

Current efficiency and capacity retention.— In the previous section we found the capacity loss rate to be characterized by $\bar{i}_{CL} = 0.12$ mA/cm^2. In order to evaluate mechanisms of loss of

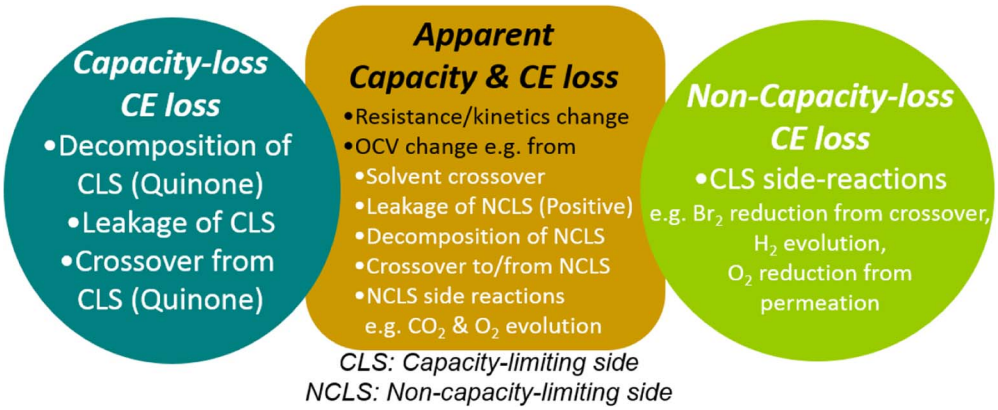

Figure 3. Loss mechanisms of current efficiency and capacity. CLS Deactivation of redox-active species on the capacity-limiting side, e.g. by decomposition, leakage, or crossover, leads directly to capacity loss and CE loss. CLS side reactions on the capacity-limiting side, such as Br_2 crossover to and reduction on the CLS, lead directly to CE loss but not to capacity loss. Both of these classes of processes, as well as NCLS side reactions on the non-capacity-limiting side, can lead, through changes induced in the OCV or kinetics, to apparent changes in CE and capacity, which may be recovered by adjusting the cycling voltage limits.

current efficiency and capacity, we identify potential mechanisms in Fig. 3 and Table I and note that some mechanisms are expected to contribute directly to both capacity loss and current efficiency loss, whereas other mechanisms are expected to contribute directly only to current efficiency loss. This categorization is related to the stoichiometric imbalance between the quinone-bearing negolyte and the bromine-bearing posolyte in our cell, assembled this way for several reasons: the anticipated bromine crossover from posolyte to negolyte, the low cost of bromine, the high corrosivity of high concentrations of Br_2 not complexed as tribromide, and to enable us to fully interrogate the properties of the novel negolyte by cycling it between 0 and 100% SOC. Other systems may also be built with stoichiometric imbalances due to cost or stability concerns, or they may develop imbalances during operation. For brevity, we term the side with the stoichiometric shortfall the "capacity-limiting side" (CLS) and the side with the stoichiometric excess the "non-capacity-limiting side" (NCLS).[c]

Capacity-loss CE-loss mechanisms.— The only mechanisms that we have identified that are expected to lead directly to both cycling capacity loss and current efficiency loss involve permanent deactivation of the redox-active species (quinone/hydroquinone) on the CLS—i.e. by quinone decomposition, by quinone/hydroquinone crossover through the membrane (which is, in principle, recoverable through rebalancing), or by CLS leakage.[d] If their equivalent current densities are i_Q^x, i_{DQ}, and i_{leak}, respectively, then

$$\bar{i}_{CL} = \bar{i}_{DQ} + \bar{i}_Q^x + \bar{i}_{leak}, \qquad [5]$$

where, unless otherwise indicated, the overbars denote averaging over a complete charge/discharge cycle throughout this paper.

Quinone crossover is very slow due to the large size and negative charge of the molecule. The permeability of AQDS through Nafion 115 was measured to be 9.0×10^{-12} cm^2/s via UV-Vis spectrophotometry. It corresponds to an equivalent current density of $\bar{i}_Q^x = 140$ pA/cm^2 in the cell—a negligible value compared to the measured value of $\bar{i}_{CL}$. The corresponding hydroquinone is assumed to exhibit a comparably low crossover rate due to its structural similarity. Quinone decomposition has been demonstrated to be insignificant under the extremely harsh conditions of boiling in a mixture of bromine and hydrobromic acid.[1] Capacity retention rates reported in a QBFB vary, but by analyzing the last 104 cycles of the 106-cycle experiment leading to the highest reported rate,[2] we infer a retention rate of 99.97% per cycle, which extrapolates to a half-life of 2,400 cycles. We assume that this report places an upper limit on the rate of molecule decomposition, represented here by an equivalent current density $\bar{i}_{DQ} \leq 0.03$ mA/cm^2 or an equivalent current of ≤ 0.15 mA. Consequently we hypothesize that the remaining mechanism—negolyte leakage (e.g. by permeation into the porous graphite flow plates), with equivalent current density i_{leak}—accounts for the balance of $\bar{i}_{CL}$ and, consequently, dominates the rate of capacity loss observed in the experiments reported here. Table I reflects our interpretation that $\bar{i}_{leak} = \bar{i}_{CL} - \bar{i}_{DQ} - \bar{i}_Q^x \approx \bar{i}_{CL}$.

Non-capacity-loss CE-loss mechanisms.— In Fig. 3 and Table I we have identified three potential CLS side reactions, which are mechanisms of CE loss that do not lead directly to capacity loss: Br_2 reduction from crossover to the CLS, H_2 evolution into the environment, and O_2 reduction due to permeation from the environment. All three of these side reactions cause the oxidation of hydroquinone to quinone, which may be reversed in the subsequent charge half-cycle. Br_2 (or Br_3^-) crossing over the membrane to the CLS and its reduction there leads to CE loss because the accompanying electrons were not forced to go through the external circuit, but it does not lead to the permanent deactivation of redox-active species in the CLS. The crossover rate through the membrane has been evaluated by measuring the reduction current with a negolyte reservoir composed of only 3 M sulfuric acid (i.e., no redox-active species) against the same posolyte used in our cycling test. At an applied potential of 0 V, a steady-state current of 6.0 mA was measured, corresponding to a cross-over loss with an equivalent current density of $\bar{i}_{Br^0}^x = 1.2$ mA/cm^2. This value is the same order of magnitude as measured in a hydrogen-bromine cell by Tucker et al.,[11] who also pointed out that the cross-over rate could be higher during cycling. Oxygen permeation through the PFA tubing is estimated using the permeation rate of 7.81×10^{-4} μg/cm/min.[12] The reduction current from such a mechanism, assuming O_2 diffusion through PFA is the rate-limiting step, is approximately 50 μA, or $\bar{i}_{O_2} = 10$ μA/cm^2. This is more than an order of magnitude lower than that of Br_2 crossover. The contribution from the hydrogen evolution reaction is neglected because the applied voltage window is considerably smaller than the kinetic water splitting window on carbonaceous materials and because a significant contribution from hydrogen evolution would cause the current efficiency to decrease with increasing current density, in contrast with the experimental observations.

It is evident from Table I that the loss of current efficiency is dominated by bromine crossover, with the next greatest contribution

[c]Our classification is distinct from the common classification of capacity losses as recoverable (e.g. vanadium crossover is recoverable by electrolyte re-balancing in a vanadium redox flow battery) or non-recoverable. In the current work, we focus on the differing impacts on cycling capacity from species losses on the CLS and on the NCLS, independent of whether the species losses are recoverable by any mechanism such as rebalancing.

[d]In principle, capacity loss without current efficiency loss would be possible with a mechanism that permanently deactivates only the low-energy form of a redox-active species during discharging of the cell, but we neglect this mechanism as implausible.

Table I. CE and Capacity Loss mechanisms. Aggregate quantities are fully capitalized.

j	Mechanism, *variable name*	Capacity loss index, g	Assumed value of f for CE loss	Equivalent current density (mA/cm^2)
1	Quinone decomposition, $\bar{i}_{DQ}$	1	$\frac{1}{2}$	$\leq$0.03
2	Quinone crossover, $\bar{i}^{x}_{Q}$	1	$\frac{1}{2}$	1.4×10^{-4}
3	Leakage, $\bar{i}_{leak}$	1	$\frac{1}{2}$	0.09–0.12
4	Bromine crossover, $\bar{i}^{x}_{Br^0}$	0	1	1.2
5	Oxygen permeation, $\bar{i}_{O_2}$	0	1	0.01
6	Hydrogen evolution, $\bar{i}_{H_2}$	0	1	Negligible
	CAPACITY LOSS, $\bar{i}_{CL}$	–	–	0.12
	CURRENT EFFICIENCY LOSS, $\bar{i}_{\mathrm{CELoss}}$	–	–	1.08

apparently coming from negolyte leakage, which is about an order of magnitude smaller.

Apparent capacity-loss & CE-loss mechanisms.— Decomposition, leakage, and side reactions occurring in the NCLS do not lead directly to capacity loss (unless the NCLS loses enough material to become the CLS on either charge or discharge). Nor do they lead directly to CE losses if they are accompanied by the planned faradaic reactions on the CLS (though a CE loss may be caused by an accompanying side reaction on the CLS). They may, however, lead to apparent changes in capacity or current efficiency if the concentration changes accompanying the loss mechanisms alter the OCV, which changes the overvoltage at which the half-cycle hits the imposed voltage limit. We term this effect *apparent changes in CE and capacity* (Fig. 3) because the charge apparently lost may be recovered by changing the cycling voltage limits. Similar effects can arise from changes in kinetic parameters such as membrane resistance, activation overvoltage for the faradaic reactions, or mass transport rates. These apparent loss mechanisms are neglected in our analysis because the voltage shift in our testing is insignificant: between the second and the last cycle at 0.25 A/cm^2, the voltage change in the early stages of a charge or discharge half-cycle (see red curves in Fig. 1b) is less than 4 mV.

Analysis of CE and capacity loss mechanisms.— Here we develop expressions for CE and capacity retention during cycling at constant current density i, in terms of the equivalent current densities of the loss mechanisms. Let $Q_{\mathrm{n-0.5}}$ be the stored charge after the n^{th} charge half-cycle occurring over a duration $t_{\mathrm{n-0.5}}$, and Q_{n} be the stored charge after the n^{th} discharge half-cycle occurring over a duration t_{n}. We assume that the cycling regimen starts with a charging half-cycle and that every charging half-cycle—including the first—starts at the same SOC. The charge stored after the n^{th} charge half-cycle is given by

$$Q_{n-0.5} = Q_{n-1} + iAt_{n-0.5} - A\bar{i}^{\mathrm{charge}}_{\mathrm{CELoss}}t_{n-0.5}, \quad [6]$$

where $\bar{i}^{\mathrm{charge}}_{\mathrm{CELoss}}$ is the time-averaged current density of current efficiency loss during the charge half-cycle. At the end of the n^{th} complete cycle, charge balance implies

$$Q_n = Q_{n-0.5} - iAt_n - A\bar{i}^{\mathrm{discharge}}_{\mathrm{CELoss}}t_n. \quad [7]$$

Using the assumption that the stored charge at the end of each cycle during cycling at constant current density is the same, we combine Equations 6 and 7 to obtain the current efficiency:

$$\overline{\mathrm{CE}} = \frac{t_n}{t_{n-0.5}} = \frac{1 - \frac{\bar{i}^{\mathrm{charge}}_{\mathrm{CELoss}}}{i}}{1 + \frac{\bar{i}^{\mathrm{discharge}}_{\mathrm{CELoss}}}{i}}. \quad [8]$$

When CE is near unity, as we observe it to be experimentally, we may expand Eq. 8 retaining only 1$^{\mathrm{st}}$ order terms in the equivalent loss currents, yielding

$$\overline{\mathrm{CE}} \approx 1 - \frac{\bar{i}^{\mathrm{charge}}_{\mathrm{CELoss}}}{i} - \frac{\bar{i}^{\mathrm{discharge}}_{\mathrm{CELoss}}}{i}. \quad [9]$$

Because, with the cycling experiments reported here, we cannot distinguish experimentally between current efficiency loss during charge and discharge half cycles, we measure only the average over a full cycle. This is related to the half-cycle values by

$$\bar{i}_{\mathrm{CELoss}} = \frac{\bar{i}^{\mathrm{charge}}_{\mathrm{CELoss}} + \bar{i}^{\mathrm{discharge}}_{\mathrm{CELoss}}}{2}. \quad [10]$$

i.e.

$$\overline{\mathrm{CE}} \approx 1 - 2\frac{\bar{i}_{\mathrm{CELoss}}}{i}. \quad [11]$$

A similar analysis can be used to address the differential capacity retention per cycle, dCR, evaluated in constant-current cycling experiments as t_n/t_{n-1}. Comparing, for the n^{th} and the $(n-1)^{\mathrm{st}}$ discharge half-cycles, charge balance equations similar to Eqs. 6 and 7 leads to

$$\mathrm{dCR} = \frac{t_n}{t_{n-1}} = \frac{\left[1 - \frac{\bar{i}^{\mathrm{charge}}_{\mathrm{CELoss}}}{i}\right]\left[1 + \frac{\bar{i}^{\mathrm{discharge}}_{\mathrm{CELoss}}}{i} - \frac{\bar{i}^{\mathrm{discharge}}_{\mathrm{CL}}}{i}\right]}{\left[1 + \frac{\bar{i}^{\mathrm{discharge}}_{\mathrm{CELoss}}}{i}\right]\left[1 - \frac{\bar{i}^{\mathrm{charge}}_{\mathrm{CELoss}}}{i} + \frac{\bar{i}^{\mathrm{charge}}_{\mathrm{CL}}}{i}\right]}, \quad [12]$$

where $\bar{i}^{\mathrm{charge}}_{\mathrm{CL}}$ and $\bar{i}^{\mathrm{discharge}}_{\mathrm{CL}}$ represent, respectively, the equivalent current densities of capacity loss during the charging and the discharging half-cycles. When dCR is near unity, as observed in our experiments, we may expand Eq. 12 retaining only 1$^{\mathrm{st}}$ order terms in the equivalent loss currents, yielding

$$\mathrm{dCR} \approx 1 - \frac{\bar{i}^{\mathrm{charge}}_{\mathrm{CL}}}{i} - \frac{\bar{i}^{\mathrm{discharge}}_{\mathrm{CL}}}{i}. \quad [13]$$

Because of the small capacity loss, a measurable value can be attained only over an extended period of cycling. Based on this value, we can calculate the average capacity loss over a single cycle, which is related to the half-cycle values by

$$\bar{i}_{\mathrm{CL}} = \frac{\bar{i}^{\mathrm{charge}}_{\mathrm{CL}} + \bar{i}^{\mathrm{discharge}}_{\mathrm{CL}}}{2}. \quad [14]$$

Thus,

$$\mathrm{dCR} \approx 1 - \frac{2\bar{i}_{CL}}{i}. \quad [15]$$

To consider the various loss mechanisms quantitatively, in Table I we list those of potential significance in our cell: quinone/hydroquinone decomposition ($j = 1$), quinone/hydroquinone crossover ($j = 2$), negolyte leakage ($j = 3$), bromine crossover and reduction ($j = 4$), O_2 permeation ($j = 5$), and H_2 evolution ($j = 6$).

We assign to each mechanism j a factor f_j that is the fraction of species lost to mechanism j that are in the high-energy ("charged") state as opposed to being in the low-energy ("discharged") state. f_j equals unity when loss mechanism j impacts only the charged species in the CLS, e.g. bromine crossover into the CLS doesn't affect the quinone but oxidizes the hydroquinone. In contrast, $f_j = \frac{1}{2}$ when the charged and discharged species in the CLS are lost equally. For example, during leakage one expects high-energy and low-energy species to be lost in proportion to their relative concentrations. In a

cell cycled symmetrically about SOC = 50%, leakage, averaged over a full cycle, corresponds to the permanent deactivation of CLS redox active species half of which are in the charged state; in such a case $f_j = \frac{1}{2}$. Because i_j and f_j can be explicit functions of i, t, or other independent variables, we analyze only the time-averaged behavior, represented by overbars. The average current efficiency loss density is given by the f-weighted sum over all mechanisms:

$$\bar{i}_{\text{CELoss}} = \sum_j \bar{f}_j \bar{i}_j. \quad [16]$$

Similarly, we assign to each mechanism j an index g_j that is unity if the mechanism contributes to capacity loss and zero if it does not. The average capacity loss current density is then given by the g-weighted sum over all mechanisms:[e]

$$\bar{i}_{\text{CL}} = \sum_j g_j \bar{i}_j. \quad [17]$$

According to Eq. 11, we interpret the parameter B in Eq. 1, and its best-fit value of 2.16 mA/cm^2, as twice the time-averaged current efficiency loss over a complete cycle. Thus $B/2$, or 1.08 mA/cm^2, has been entered for the aggregate $\bar{i}_{\text{CELoss}}$ into Table I. The agreement of the fitted curve to the data in Fig. 2b is interpreted as evidence that the most significant CE loss mechanisms occur at rates that are not significantly dependent on applied current density. According to this interpretation, $B/2$ should equal the f-weighted sums of the six equivalent current densities reported in Table I. The agreement is good, to within 20%.

From Eq. 15, the capacity retention over N cycles is

$$\text{CR} = \left(1 - \frac{2\bar{i}_{CL}}{i}\right)^{N-1}. \quad [18]$$

We evaluated $\bar{i}_{\text{CL}}$ from our measurements using Eq. 2. As the experiments reported here do not provide the resolution to quantify the dependence of capacity retention on current density, we instead report an effective value that the differential capacity retention would take, dCR_{eff}, for a comparable cell if it cycled only at the base current density (0.25 mA/cm^2) after the same t_{tot}. Dividing t_{tot} with the average cycle time gives us an effective cycle number, $N_{eff} = 29.8 \approx 30$. Eqs. 15 and 18 yield a dCR_{eff} of 99.90% and a CR_{eff} of 97.1% after 30 effective cycles. Note that, if our hypothesis is correct that the capacity loss rate is independent of applied current density, then Eq. 15 predicts the differential capacity retention rate for all current densities. This hypothesis is testable with more extensive cycling experiments than those reported here.

Lessons learned.— The above analysis highlights factors that impact each aspect of the cell cycling performance. The current efficiency, which is dominated by Br_2 crossover, trades off against the voltage efficiency. The crossover rate for the cell studied here has been reduced compared to in previous work[1] by using a thicker, untreated membrane.[f]

The crossover rate has also been reduced by employing a large HBr/Br_2 ratio, so that most of the Br_2 complexes with Br^- to form Br_3^-, which is repelled electrostatically from the negatively-charged functional groups in the membrane. Employing a large molar excess of HBr-laden posolyte over negolyte also cuts the crossover rate by keeping the Br_2 concentration low even when the cell is fully charged. All of these modifications, however, decrease the voltage efficiency: a thick membrane leads to a larger r_p; a high HBr concentration lowers the OCV, and a large molar excess of posolyte keeps the HBr concentration high even at intermediate and high negolyte states of charge. We note that bromine crossover should ultimately render the positive side capacity-limiting, after a time period of

$$t = \frac{(\Delta - 1)\, C_{\text{CLS}}}{\bar{i}^{\text{x}}_{\text{Br}^0} A} \quad [19]$$

where Δ is the charge capacity ratio of the NCLS over CLS, C_{CLS} is the charge capacity of the CLS, $\bar{i}^{\text{x}}_{\text{Br}^0}$ is the crossover current density of oxidized bromine (i.e., that arising from Br_2 and Br_3^- crossover), and A is the membrane-electrode assembly area. In the cell reported here, with $\bar{i}^{\text{x}}_{\text{Br}^0} = 1.2$ mA/cm^2 and $C_{\text{CLS}} = 4824$ C, this transition should not occur until about 80 days. But before reaching this turning point, other associated electrolyte changes, such as pH change and water transport, could have already severely degraded cell performance. These factors underscore the importance of membrane selectivity. In practical usage, the actual crossover rate will depend on how the battery is utilized, and may be greatly reduced when the battery is idle.

Among the various mechanisms of loss of current efficiency that we have identified, the three that are expected to lead directly to capacity loss with cycling are leakage of the electrolyte containing the smaller charge capacity (the quinone-bearing negolyte), destruction of redox-active species in this electrolyte, and crossover of redox-active species from this electrolyte. The magnitude of the current inefficiency leading to capacity loss is approximately 0.61 mA, or 0.12 mA/cm^2. The quinone crossover rate has been shown to be insignificant. Although a very small amount of leakage can be significant in a very small cell, leakage is not anticipated to be important in well-engineered scaled-up flow batteries. In contrast, molecule destruction would be a much more significant problem. Although prior work has shown AQDS to be exceedingly stable to exposure to boiling mixtures of bromine and hydrobromic acid,[1] it will be important to place rigorous upper limits on the decomposition rate in an operating cell.

Conclusions

1. The QBFB examined here, with interdigitated flow fields, exhibits linear polarization curves except at current densities exceeding 0.25 A/cm^2 when discharging at 10% SOC or charging at 90% SOC.
2. The decrease in cycle capacity with increasing current density is accounted for quantitatively via the interplay of the polarization curves and the voltage limits imposed during cycling. Higher current density causes higher overvoltage and the cell thereby reaches a voltage limit sooner.
3. The linearity of the polarization curves leads to the instantaneous voltage efficiency being inversely related to the ratio of current density to short-circuit current density, as described by Eq. 4, $VE = \frac{2}{1+\frac{i}{i_{SC}}} - 1$.
4. The same relationship exists between average voltage efficiency during cycling and current density, if the OCV and polarization resistance are evaluated at 50% SOC. Thus, for any RFB exhibiting linear polarization curves, $\overline{\text{VE}} \geq 0.9$ or $\overline{\text{VE}} \geq 0.8$ requires that the applied current density not exceed approximately 6% or 11% of i_{sc}, respectively.
5. The current efficiency is a function of i and $\bar{i}_{\text{CELoss}}$ given by Eq. 8, which Taylor expands to Eq. 11, $\overline{\text{CE}} \approx 1 - 2\bar{i}_{\text{CELoss}}/i$.
6. Individual loss mechanisms contribute to CE loss and to capacity loss with different weighting factors, f_j and g_j respectively, as indicated in Table I.
7. The major source of loss of current efficiency is Br_2 crossover, occurring at a rate of 1.2 mA/cm^2.
8. The ratio of this crossover rate, presumed to be constant, to the applied current density leads to a current efficiency that increases with increasing current density in a manner that is quantitatively consistent with experiment.
9. The differential capacity retention is a function of i and i_{CL} given by Eq. 12, which Taylor expands to Eq. 15, $\text{dCR} \approx 1 - 2\bar{i}_{CL}/i$. The average rate of capacity loss is 0.61 mA or 0.12 mA/cm^2.
10. To obtain an effective value of the differential capacity retention rate for the cell undergoing cycling at multiple current densities,

[e]We note that even though Table I indicates a correlation between the values of f and g, this is not necessarily always the case.

[f]The Br_2 crossover current density through a Nafion 212 membrane pre-treated as in Ref. 8 is about 3.25 mA/cm^2.

a comparison cell cycling at constant current density for the same total duration leading to the same cumulative capacity retention is analyzed. The effective differential capacity retention is 99.90% per cycle.

11. Among the various mechanisms of loss of current efficiency that we have identified, leakage of the minority electrolyte— the quinone-bearing negolyte—crossover and destruction of redox-active species in this electrolyte are the three that are expected to lead directly to capacity loss with cycling. We interpret prior work on QBFB cycling stability to imply that the molecule destruction rate is no more than approximately one-quarter of the total and quantify its crossover rate to be three orders of magnitude smaller; the balance is provisionally assigned to leakage.

Acknowledgments

This research was supported partially by the US Department of Energy ARPA-E Award DE-AR0000348 and partially by the Harvard School of Engineering and Applied Sciences. We thank Michael Gerhardt, Michael Marshak and Andrew Wong for insightful discussions.

References

1. B. Huskinson, M. P. Marshak, C. Suh, S. Er, M. R. Gerhardt, C. J. Galvin, X. Chen, A. Aspuru-Guzik, R. G. Gordon, and M. J. Aziz, *Nature*, **505**, 195 (2014).
2. B. Huskinson, M. P. Marshak, M. R. Gerhardt, and M. J. Aziz, *ECS Trans.*, **61**, 27 (2014).
3. B. Yang, L. Hoober-Burkhardt, F. Wang, G. K. Surya Prakash, and S. R. Narayanan, *J. Electrochem. Soc.*, **161**, A1371 (2014).
4. F. Y. Fan, W. H. Woodford, Z. Li, N. Baram, K. C. Smith, A. Helal, G. H. McKinley, W. C. Carter, and Y.-M. Chiang, *Nano Lett.*, **14**, 2210 (2014).
5. T. Nguyen and R. F. Savinell, *Electrochemical Soc. Interface*, **19**(3), 54 (2010).
6. M. Skyllas-Kazacos, M. H. Chakrabarti, S. A. Hajimolana, F. S. Mjalli, and M. Saleem, *J. Electrochem. Soc.*, **158**, R55 (2011).
7. A. Z. Weber, M. M. Mench, J. P. Meyers, P. N. Ross, J. T. Gostick, and Q. Liu, *J. Appl. Electrochem.*, **41**, 1137 (2011).
8. Q. Chen, M. R. Gerhardt, L. Hartle, and M. J. Aziz, *J. Electrochem. Soc.*, **163**, A5010 (2016).
9. R. M. Darling and M. L. Perry, *J. Electrochem. Soc.*, **161**, A1381 (2014).
10. D. Aaron, Z. Tang, A. B. Papandrew, and T. A. Zawodzinski, *J. Appl. Electrochem.*, **41**, 1175 (2011).
11. M. C. Tucker, K. T. Cho, F. B. Spingler, A. Z. Weber, and G. Lin, *J. Power Sources*, **284**, 212 (2015).
12. www.kynar.com.
13. K. T. Cho, M. C. Tucker, M. Ding, P. Ridgway, V. S. Battaglia, V. Srinivasan, and A. Z. Weber, *Chempluschem*, **80**, 402 (2014).